RSC Advances

PAPER

View Article Online
View Journal | View Issue

Cite this: *RSC Adv.*, 2015, **5**, 36656

One-step synthesis of copper compounds on copper foil and their supercapacitive performance

Panpan Xu, Ke Ye,* Mengmeng Du, Jijun Liu, Kui Cheng, Jinling Yin, Guiling Wang and Dianxue Cao*

Received 19th March 2015
Accepted 15th April 2015

DOI: 10.1039/c5ra04889c

www.rsc.org/advances

Nanowire-like $Cu(OH)_2$ arrays, microflower-like CuO standing on $Cu(OH)_2$ nanowires and hierarchical CuO microflowers are directly synthesized *via* a simple and cost-effective liquid–solid reaction. The specific capacitance of $Cu(OH)_2$, $CuO/Cu(OH)_2$ and CuO are 511.5, 78.44 and 30.36 F g^{-1}, respectively, at a current density of 5 mA cm^{-2}. Therefore, the $Cu(OH)_2$/Cu-foil electrode displays the best supercapacitive performance. The capacitance retention reaches up to 83% after 5000 charge/discharge cycles with the columbic efficiency of ~98%. More importantly, the nanowire $Cu(OH)_2$ transformed into stable nanosheet CuO after about 600 constant current charge–discharge cycles. Additionally, we fabricate an asymmetric supercapacitor with nanowire $Cu(OH)_2$/Cu-foil as a positive electrode, activated carbon (AC) as a negative electrode and 6 mol dm^{-3} KOH as electrolyte, which exhibits an energy density of 18.3 W h kg^{-1} at a power density of 326 W kg^{-1}.

1. Introduction

With the rapid development of the global economy, the exhaustion of fossil fuels and increasing environmental pollution, there is an urgent need for efficient, clean, and sustainable sources of energy, as well as new technologies related to energy conversion and storage.[1–3] In this context, supercapacitors comprising a characteristic combination of high power and reasonable energy density with faster response time and near-infinite life cycle can complement other energy storage devices like conventional capacitors, batteries and fuel cells.[4,5]

According to the charge storage mechanism, supercapacitors are classified into two types: (i) electrochemical double layer capacitors (EDLCs) which stores the energy non-Faradically by the accumulation of the charges at the electrode–electrolyte interface and (ii) redox capacitors which stores the energy Faradically by battery-type oxidation reduction reactions leading to the pseudocapacitive behavior.[6] The EDLCs usually use carbon-based materials (activated carbons, carbon nanotubes, templated carbons, carbide-derived carbons, carbon fibers, carbon aerogels and graphene).[7–10] Carbon materials have limited specific due to their double-layer charge storage mechanism. To improve the specific capacitance of supercapacitors, lots of researches have been dedicated to the investigation of metal oxides or hydroxides pseudocapacitive materials. One promising candidate is RuO_2, which has a specific capacitance reported to be as high as to 1340 F g^{-1}, but RuO_2 is very expensive.[11,12] Therefore, cost-effective transition metal oxides or hydroxides, such as $Ni(OH)_2$,[13,14] $Co(OH)_2$,[15,16] MnO_x,[17,18] CuO,[19–21] Fe_2O_3,[22–24] V_2O_5,[25,26] and SnO_2,[27,28] has been widely investigated. Among the possible materials for pseudocapacitors, cupric oxides have attracted significant attention in recent years due to their promising high specific capacitance, environmentally friendly nature, and the low cost. Therefore, many research groups have been considering cupric oxides or hydroxides as a supercapacitor electrode recently, a brief summary of which is in Table 1.[21,29–32] To our knowledge, studies on the supercapacitive behavior of $Cu(OH)_2$ is rear and only one report showed that $Cu(OH)_2$ displayed a specific capacitance of 120 F g^{-1}.[33]

Recent years have witnessed great progress in the design of additive/binder-free electrode architectures to avoid the "dead surface" in traditional slurry-derived electrode and allow for more efficient charge and mass exchange. Different types of conductive substrates (*e.g.*, Ni foam, Ti foil, stainless-steel foil, and flexible graphite paper) are used as current collector for electrochemical supercapacitor.[34–37] Nanostructured electroactive materials prepared by *in situ* oxidation of copper foil would not only improve the charge transfer but also reduce the internal resistance and maintain a rapid redox reaction.

Herein, nanowire-like $Cu(OH)_2$ arrays, microflowers-like CuO standing on $Cu(OH)_2$ nanowire and hierarchical CuO microflowers were directly grown onto copper foil *via* surface oxidation in alkaline solution to obtain a conducting additive-free and binderless electrode with high utilization of the active material. The supercapacitive performance of the obtained electrode were evaluated. This nanowire structured

Key Laboratory of Superlight Materials and Surface Technology of Ministry of Education, College of Materials Science and Chemical Engineering, Harbin Engineering University, Harbin, 150001, P.R. China. E-mail: yeke@hrbeu.edu.cn; caodianxue@hrbeu.edu.cn

Table 1 Summery of electrochemical data of CuO and $Cu(OH)_2$ based electrodes

Morphology	Current density or scan rate	C_s (F g^{-1})	Stability	Ref.
Nanosheet	5 mA cm^{-2}	569	17.5% loss (5000 cycles)	21
Nanosheet	0.41 A g^{-1}	212	15% loss (800 cycles)	20
Nanoflower	10 mA cm^{-2}	134	5.2% loss (200 cycles)	43
Nanoflower	0.41 A g^{-1}	159	5% loss (850 cycles)	20
Nanoflake	2 mA cm^{-2}	190	33% loss (2000 cycles)	40
Lotus-like CuO/$Cu(OH)_2$	2 mA cm^{-2}	278	15% loss (800 cycles)	29
Nanostructure	2 mA cm^{-2}	162	19% loss (2000 cycles)	44
Cautiflower	0.41 A g^{-1}	102	15% loss (850 cycles)	20
Nanowire	2 mV s^{-1}	88.5	9.4% loss (500 cycles)	45
Nanosheet	2 A g^{-1}	340	15% loss (2000 cycles)	46
Nanobelt	1 A g^{-1}	130	30% loss (7000 cycles)	47
Nanoflower	3 mA cm^{-2}	137	12% loss (500 cycles)	48
Nanoribbon	5 mV s^{-1}	346	18% loss (5000 cycles)	33
Nanograin ($Cu(OH)_2$)	10 mV s^{-1}	120	Not available	36
Nanowire ($Cu(OH)_2$)	2 mA cm^{-2}	750	17% loss (5000 cycles)	This work

$Cu(OH)_2$ with 6 M KOH electrolyte shows the best supercapacitive performance. Since the cross wire-like architecture provides good electrical conductivity, effective electrolyte-accessible channels for ion transportation. Our results demonstrate that the present cost-effective $Cu(OH)_2$ nanowires could be a choice for supercapacitor electrode materials characterized by their high specific capacitance and related properties. Moreover, an asymmetric supercapacitor was obtained by using the $Cu(OH)_2$/Cu-foil and activated carbon (AC) as the positive and negative electrodes, respectively.

2. Experimental

2.1. Preparation and characterization of positive electrode

All the chemicals are of analytical grade and were used without further purification. The schematic illustration of the experimental setup is shown in Fig. 1a, which is confirmed by the extra experiments below. A fresh Cu foil (0.15 mm, 99.95%, Tianjin Hengxing Chemical Preparation Co., Ltd China) was cut into 1 cm × 1 cm sheet (Fig. 1b). It was cleaned by a consecutive ultrasonication in acetone, ethanol, distilled water for 10 min, and then put it into 1.0 mol dm^{-3} HCl solution to remove any surface impurities and oxide layers. The surface of the copper foil became bright and smooth after treatment (Fig. 1c). One side of the copper foil was coated by nail enamel. The pre-cleaned Cu foil was then immersed in an aqueous solution consisting of 12 mL NaOH (10 mol dm^{-3}), 6 mL $(NH_4)_2S_2O_8$ (1.0 mol dm^{-3}) and 27 mL distilled water. A few minutes later, the exposed copper foil surface turned to a faint blue color, and the initial colorless solution became increasingly blue. The reaction time of copper in the solution were 30 min (Fig. 1d), 60 min (Fig. 1e) and 120 min (Fig. 1f), respectively. The electrodes were all then rinsed with water and ethanol, and dried in air after extracted from the solution.

The morphology was examined by scanning electron microscope (SEM, JEOL JSM-6480) and transmission electron microscope (TEM, FEI Teccai G2 S-Twin, Philips). The crystallographic phases of all the sample were investigated by X-ray diffractometer (XRD, Rigaku TTR III) with Kα radiation (λ = 0.1506 nm) with a scan rate of 10° min^{-1} at a step width of 0.02°.

2.2. Preparation of AC electrode

The AC negative electrode was prepared by mixing 80 wt% of activated carbon (2000 ± 100 m^2 g^{-1}), 10 wt% acetylene black and 10 wt% polyvinylidene difluoride (PVDF) binder in *N*-methyl-2-pyrrolidone (NMP). The obtained thick paste was coated onto 1.0 cm × 1.0 cm carbon fiber cloths (CFC) and dried in 100 °C vacuum oven. Prior to use CFC, the CFC was degreased with acetone for 15 min, rinsed again with water extensively, and dried in air.

2.3. Electrochemical measurements

The electrochemical tests were carried in a conventional three-electrode electrochemical cell using a computerized

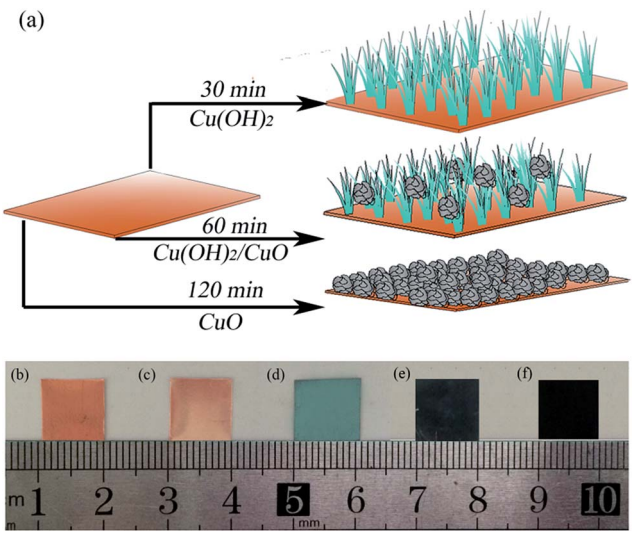

Fig. 1 Schematic diagram of $Cu(OH)_2$/Cu-foil electrode (a); photographs of Cu foil (b); the Cu foil after pretreatment (c); $Cu(OH)_2$/Cu-foil electrode (d); CuO/$Cu(OH)_2$/Cu-foil electrode (e); CuO/Cu-foil electrode (f).

potentiostat (VMP3/Z Bio-Logic) controlled by the EC-lab software. The as-prepared electrode (1 × 1 cm^2 nominal planar area) acted as the working electrode, a platinum foil (1 × 2 cm^2) served as the counter electrode, and a saturated calomel electrode (SCE) was used as the reference electrode. The asymmetric supercapacitor using nanosheet CuO/Cu-foil as positive and AC as negative electrode was tested in two-electrode electrochemical cell. The cycle life tests were conducted on a Land battery program-control test system. All electrochemical measurements were performed in 1.0 mol dm^{-3} KOH electrolyte. The solutions were made with analytical grade chemical reagents and Milli-Q water (18 MΩ cm, Millipore). EIS measurements were performed by applying an alternating voltage with 5 mV amplitude in a frequency range from 0.01 Hz to 100 kHz at the open circuit potential.

3. Results and discussion

3.1. Characterization of electrodes

XRD analysis was first performed to study the crystal structure of the electrodes. As shown in Fig. 2, the strong diffraction peak marked with heart-shape comes from the Cu substrate (JCPDS file no. 04-0836). The diffraction peaks marked with cinquefoil and rhombus can be indexed to orthorhombic $Cu(OH)_2$ (JCPDS file no. 80-056) and monoclinic CuO (JCPDS file no. 80-1916) perfectly. This indicates that the pure $Cu(OH)_2$, $Cu(OH)_2$/CuO composites and pure CuO were successfully synthesized on copper foil at reaction time of 30 min, 60 min and 120 min, respectively. The $Cu(OH)_2$, $Cu(OH)_2$/CuO and CuO nanostructure could be formed on Cu substrate by the surface oxidation of copper in alkaline solution as expressed by the following equation according to literature.[38]

$$Cu + 4NaOH + (NH_4)_2S_2O_8 \xrightarrow{30\ min} Cu(OH)_2 + 2Na_2SO_4 + 2NH_3\uparrow + 2H_2O \quad (1)$$

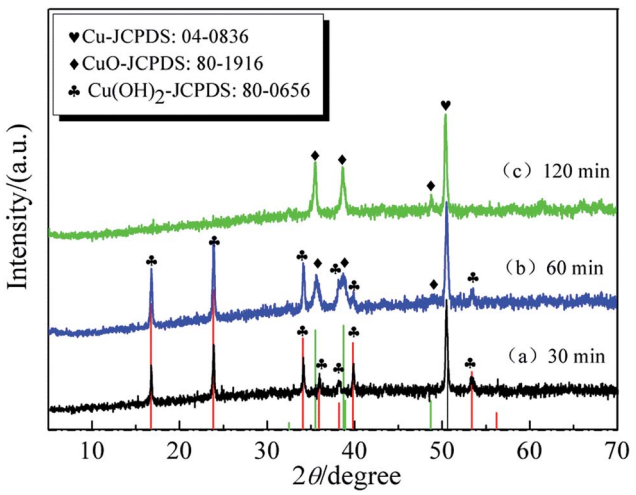

Fig. 2 XRD patterns of the $Cu(OH)_2$/Cu-foil electrode, CuO/$Cu(OH)_2$/Cu-foil electrode and CuO/Cu-foil electrode.

$$2Cu + 8NaOH + 2(NH_4)_2S_2O_8 \xrightarrow{60\ min} CuO + Cu(OH)_2 + 4Na_2SO_4 + 4NH_3\uparrow + 5H_2O \quad (2)$$

$$Cu + 4NaOH + (NH_4)_2S_2O_8 \xrightarrow{120\ min} CuO + 2Na_2SO_4 + 2NH_3\uparrow + 3H_2O \quad (3)$$

The surface morphologies of the electrodes were investigated by SEM. Fig. 3a shows the SEM image of the copper foil after pre-treated. At the reaction time of 30 min, the $Cu(OH)_2$ forms a blue thick film and covers the entire copper substrate uniformly and compactly at low magnification (Fig. 3b). The higher magnification SEM image (Fig. 3c) reveals that the film is composed of nanowires, many of them then assemble to form a cluster which crosses each other. Fig. 3d is the TEM image of a single $Cu(OH)_2$ nanowire scratched down from the copper foil. The length of a single nanowire is up to around 4.6 μm with the width about 330 nm. At the reaction time of 60 min, the hierarchical structures of CuO appears, as shown in Fig. 3e and f. The flower-like CuO microspheres are evident with a diameter of 3–5 μm uniformly (Fig. 3e). The magnified image of a single

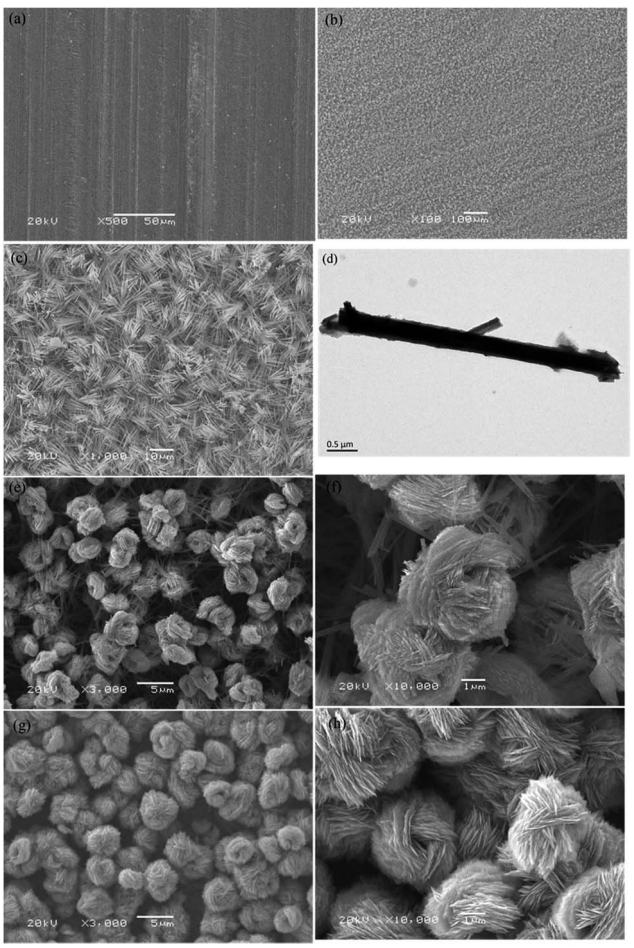

Fig. 3 SEM images and TEM images of pre-cleaned Cu foil (a), $Cu(OH)_2$/Cu-foil electrode (b) (c) (d); CuO/$Cu(OH)_2$/Cu-foil electrode (e) and (f); CuO/Cu-foil electrode (g) and (h).

microflower (Fig. 3f) reveals that the thickness of the flower petals is approximately 50–100 nm. Interestingly, the microflowers CuO are standing on $Cu(OH)_2$ nanowire arrays. At the reaction time of 120 min, Fig. 3g and h show that the $Cu(OH)_2$ nanowires disappear and the CuO presented as the uniform microflowers covering the Cu substrate. The longer reaction time did not change the morphology of CuO, but did increase the amount of microflowers.

3.2. Electrochemical properties of electrodes

Capacitor performance of electrodes could be evaluated with cycle voltammogram (CV) and galvanostatic charge–discharge (GCD) measurements. Fig. 4a summarizes the results of the CV studies of the $Cu(OH)_2$/Cu-foil electrode, CuO/$Cu(OH)_2$/Cu-foil electrode and CuO/Cu-foil electrode (all have the same geometrical area of 1 cm^2) at a scan rate of 2 mV s^{-1} in 6.0 M KOH solution. The CV profiles for all the three samples are quite different from the ideal rectangular shape for double layer capacitance indicating that the electrodes possess pseudocapacitance properties. The specific capacitance of the samples could be estimated from the cathodic or anodic part of the CV data using the equation:

$$C_s = \frac{1}{mv(E_2 - E_1)} \int_{E_1}^{E_2} i(E)\mathrm{d}E \quad (4)$$

where E_1 and E_2 are the cutoff potentials in the CV curves and $i(E)$ is the current at each potential, $E_2 - E_1$ is the potential window, v is the scan rate and m is the mass of the active materials. In this report, the mass loading of $Cu(OH)_2$, CuO/$Cu(OH)_2$, CuO on Cu substrate is around 0.7, 1.6 and 2.1 mg cm^{-2}. The specific capacitance for $Cu(OH)_2$/Cu-foil electrode, CuO/$Cu(OH)_2$/Cu-foil electrode, CuO/Cu-foil electrode based on CV curves are 65.3, 153 and 685 F g^{-1}. Therefore, the $Cu(OH)_2$/Cu-foil electrode displays the best supercapacitive property compared with the other two electrodes.

Apparently, when the voltage is beyond 0.4 V, the system occurs oxygen evolution phenomenon, thus the GCD measurement was tested in the potential window of 0–0.4 V in 6 M KOH (Fig. 4b) at 5 mA cm^{-2}. The obvious non-linear shape of the discharge curves further reveal that the capacitance of electrodes are not pure double-layer capacitance, but a pseudocapacitance, involving a faradic capacitance, which mainly originates from the redox reactions. The specific capacitance of the electrodes can be calculated from the discharge curves using the following equation:

$$C_m = \frac{I_d \times \Delta t}{\Delta V \times m} \quad (5)$$

where C_m (F g^{-1}) is the specific capacitance, I_d (mA) is the discharge current, Δt (s) is the discharge time, ΔV (V) is the discharge potential range, and m (mg) is the mass of active materials. The specific capacitance values of $Cu(OH)_2$/Cu-foil electrode, CuO/$Cu(OH)_2$/Cu-foil electrode, CuO/Cu-foil electrode are 511.5, 78.44 and 30.36 F g^{-1} which is in good agreement with the CV curves (Fig. 4a). The potential drop between the charge and discharge curves (IR drop) is generally caused by internal resistance and incomplete faradic reaction in the electrode. The difference in supercapacitive performance of the three electrodes majorly arise from their distinctive morphology. On one hand, the cross nano-sized wire-like $Cu(OH)_2$ provide larger electrode–electrolyte interface for efficient redox reaction than micro-sized flower-like CuO. On the other hand, since one-dimensional morphologies posses the property of directional charge transport, the nanowire $Cu(OH)_2$ display lower charge transfer resistance (see Fig. 7) and smaller IR drop than microflower CuO.

Fig. 5a shows the CVs of the $Cu(OH)_2$/Cu-foil electrode recorded in 6 M KOH solution at various scan rates. The CV curves show lower slopes for lower scan rates, which indicates that lower scan rates allow a longer duration for the anions to access the bulk of the electrode; thereby showing ideal capacitive behavior. However, with increasing scan rate the anodic peak shifts towards positive potentials and the cathodic peak shifts towards negative potentials as has been observed conventionally. This demonstrates the quasi-reversible nature

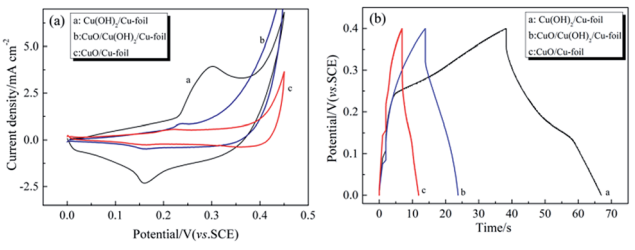

Fig. 4 CV curves of $Cu(OH)_2$/Cu-foil electrode, CuO/$Cu(OH)_2$/Cu-foil electrode and CuO/Cu-foil electrode in 6 M KOH electrolyte at a scan rate of 2 mV s^{-1} (a); the charge–discharge curves of $Cu(OH)_2$/Cu-foil electrode, CuO/$Cu(OH)_2$/Cu-foil electrode and CuO/Cu-foil electrode in 6 M KOH electrolyte at a current density of 5 mA cm^{-2} (b).

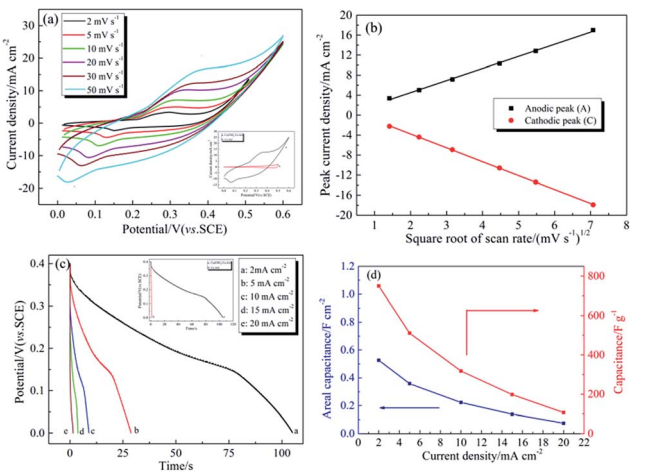

Fig. 5 CV curves of $Cu(OH)_2$/Cu-foil electrode in 6 M KOH electrolyte at different scan rates (a); voltammetric current as a function of square root of scan rate in 6 M KOH electrolyte (b); discharge curves of $Cu(OH)_2$/Cu-foil electrode at different current densities in 6 M KOH electrolyte (c); variation of specific capacitance as a function of current density in 6 M KOH electrolyte (d).

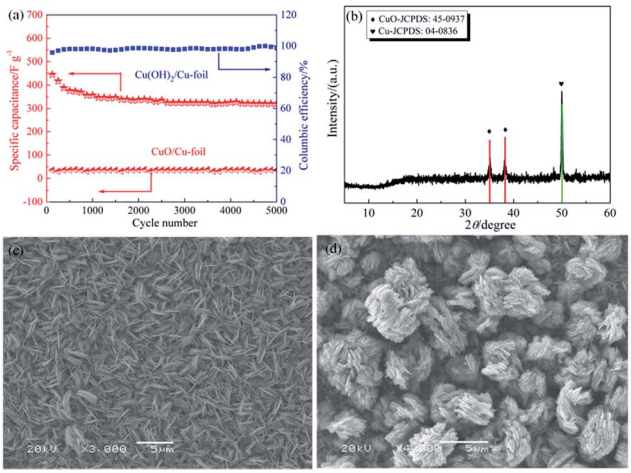

Fig. 6 Dependences of the discharge specific capacitance and the columbic efficiency on the charge/discharge cycle numbers at current density of 5 mA cm^{-2} in 6 M KOH electrolyte for $Cu(OH)_2$/Cu-foil and CuO/Cu-foil electrodes(a). The XRD (b) and SEM images for $Cu(OH)_2$/Cu-foil (c) and CuO/Cu-foil (d) electrodes after cycling.

of redox reaction. From the inset of Fig. 5a, it can be seen that the capacitive current of Cu-foil substrate is significantly lower than that of $Cu(OH)_2$/Cu-foil electrode, suggesting that the capacitance contribution of the Cu-foil substrate to the $Cu(OH)_2$/Cu-foil electrode can be neglected. All the plots show the oxidation (anodic) and reduction (cathodic) events indicative of the pseudocapacitance charge storage mechanism. Based on literatures reporting about redox of CuO and $CuO/Cu(OH)_2$ composites in aqueous electrolytes,[19,32,39–41] within the potential range of 0–0.6 V, the following reactions between Cu(I) and Cu(II) species (eqn (2) and (3)) might exist.

$$2Cu(OH)_2 + 2e^- \Leftrightarrow Cu_2O + 2OH^- + H_2O \quad (6)$$

$$Cu_2O - 2e^- + 2OH^- \Leftrightarrow 2CuO + H_2O \quad (7)$$

The anodic peak A appearing can be attributed to the oxidation of Cu_2O to CuO and $Cu(OH)_2$. The cathodic peak C can be ascribed to the reduction of CuO and $Cu(OH)_2$ to Cu_2O. Previous studies have shown that the reduction of $CuO/Cu(OH)_2$ to Cu and the oxidation of $CuO/Cu(OH)_2$ to Cu(III) species do not occur in the 0–0.6 V potential range.[42,43] It should be pointed out that the CVs shown in Fig. 5a are the stabilized curves after around 5 potential cycles, during which $Cu(OH)_2$ originally formed on copper foil was partially reduced to Cu_2O. The oxidation of this Cu_2O generated the anodic peak (A). Besides, the $Cu(OH)_2$/Cu-foil electrode did not show supercapacitive property when tested the CVs in neutral electrolyte, such as Na_2SO_4, K_2SO_4, Li_2SO_4. This result indicates that the abundant OH^- is necessary when $Cu(OH)_2$ undergoes redox reaction as a pesudocapacitive material (according to eqn (6) and (7)).

In pseudocapacitive materials, such as $Cu(OH)_2$, the anodic peak current (i_{pa}) and cathodic peak current (i_{pc}) against $v^{1/2}$ is analyzed to determine whether the capacitance originates from surface redox reactions or from bulk diffusion. Fig. 5b shows a nearly linear relationship, which implies that the electrode reaction is diffusion-controlled with the electrolyte involved.

Additionally, constant current charge–discharge curves at various current densities were performed in 6.0 mol dm^{-3} KOH solution to further evaluate the electrochemical performance of the $Cu(OH)_2$/Cu-foil electrode (Fig. 5c). The specific capacitance values of the $Cu(OH)_2$ evaluated from the discharge curves according to eqn (5) are 750, 511, 318, 198, and 107 F g^{-1} at the current density of 2, 5, 10, 15 and 20 mA cm^{-2}, respectively. Obviously, compared with the findings (Table 1), the electrospun copper oxide nanowire powder prepared by Vidhyadharan *et al.*[39] shows the highest specific capacitance (620 F g^{-1} at the current density of 2 A g^{-1}). However, the specific capacitance of our $Cu(OH)_2$ nanowire structure directly grown on copper foil mentioned here is much higher than that (750 F g^{-1} at the current density of 2.86 A g^{-1}). The possible reasons for the superior capacitance can be attributed to three aspects: (i) the $Cu(OH)_2$/Cu-foil electrode fabricated by the directly oxidation of copper foil avoiding using of conductive agent and binder which reduces the resistance efficiently; (ii) the unique uniform nanowires interconnected with each other generating abundant space which enable the electrolyte easier further diffuse to the nanowire surface and thus reduce the concentration polarization; (iii) one-dimensional morphologies of nanowire possess the property of directional charge transport promoting fast electron transfer, which weaken the electrochemical polarization. In order to further clarify the effect of Cu-foil substrate on the capacitance performance, the galvanostatic discharge curves of the Cu-foil substrate and the $Cu(OH)_2$/Cu-foil electrode with the same geometrical area of 1 cm^2 were compared in inset of Fig. 5c. The discharge time of the Cu-foil substrate is only 0.36 s, which can be ignored compared to that of the $Cu(OH)_2$/Cu-foil electrode (105 s). Besides, the surface area of Cu foil substrate in the $Cu(OH)_2$/Cu-foil electrode was completely covered by $Cu(OH)_2$. These results (inset of Fig. 5a and c) displayed that the Cu foil substrate could not bring about substantial contribution to the specific capacitance of $Cu(OH)_2$/Cu-foil electrode. The performance of an asymmetric capacitor employing $Cu(OH)_2$/Cu-foil as one of the electrodes is not reported herein; the purpose of the present paper is a thorough understanding of the electrochemical properties of $Cu(OH)_2$ nanowires.

The specific capacitance of $Cu(OH)_2$ is plotted as a function of the current density in Fig. 5d. The specific capacitance decreased with increasing current density. When the discharge current density increases from 2 mA cm^{-2} (2.86 A g^{-1}) to 20 mA cm^{-2} (28.6 A g^{-1}), the specific capacitance of $Cu(OH)_2$/Cu-foil electrode decreases from 750 F g^{-1} to 107 F g^{-1}. The noteworthy decrease in capacitance is possibly the result of the increased potential drop caused by the electrode resistance and the relatively in sufficient Faradic redox reaction under high current densities. This phenomenon can be explained clearly by Fig. 5b. Generally, the majority of the active surface is utilized by the ions for charge storage at the lower current density, thereby resulting in the higher specific capacitance. The ion movement is limited only to the surfaces of the electrode material at higher

current density when electrochemical double layer capacity is the dominant mechanism. Therefore, the contribution from the bulk diffusion is no longer available and the specific capacitance drops off drastically. Impurity doping or addition of carbon nanotubes are possible routes to further improve the rate capability of the $Cu(OH)_2$/Cu-foil electrode.

Long cyclic stability is an important requirement for practical competence of supercapacitor devices. The cyclability of the $Cu(OH)_2$/Cu-foil electrode was investigated by continuous charge/discharge measurements over 5000 cycles (Fig. 6a). The study was performed at a current density of 5 mA cm^{-2} (7.14 A g^{-1}) in 6.0 M KOH solution within the potential range of 0–0.4 V. The specific capacitance decreased by 17% during the first 600 cycles, after which it was almost constant at approximately 360 F g^{-1} for up to 5000 cycles. The possible reason for the decrease of capacitance may involve microstructure change and resistance increase (see Fig. 7). The morphology and structure of the electrode after 600 cycles were examined by scanning electron microscopy and X-ray diffraction spectroscopy. The XRD analysis result (Fig. 6b) shows that all the diffraction peaks marked with rhombus fit well to monoclinic CuO (JCPDS card no. 45-0937) with different lattice parameters from the microflower CuO prepared in this report (see Table 2). The diffraction peak at 50.4° comes from the copper foil (JCPDS card no. 04-0836). In other words, during charging, the Cu_2O undergoes a oxidation process turning into $Cu(OH)_2$ and CuO (eqn (6) and (7)). Fig. 6c shows the SEM image of the $Cu(OH)_2$/Cu-foil electrode after 600 cycles, which implies that the original nanowire arrays have turned into nanosheets completely with a diameter of about 1 μm during the repetitive charge/discharge cycling. Apparently, since the space between the nanosheet CuO is much smaller than nanowire $Cu(OH)_2$, it is difficult for electrolyte to further diffuse. Consequently, the utilization of nanowire $Cu(OH)_2$ is higher than nanosheet CuO which causes the electrochemical performance of the $Cu(OH)_2$ is superior than the CuO. Compared with the previous CuO microflower mentioned in this article, on account of the formation of the former microflowers is the result of the aggregation of nanosheets (see Fig. 3g and h), the charge transfer and electrolyte diffusion resistance of the microflower CuO is larger (see Fig. 7) which leads to its capacity is smaller than the present nanosheet CuO. In addition, Fig. 6a shows the capacitance retention of microflower CuO/Cu-foil is nearly 100% during 5000 charge–discharge cycles, which may results from the unchanged morphology (Fig. 6d). This phenomenon indicates the morphology of the active materials has great influence on the electrochemical property. The columbic efficiency was calculated using the following equation

$$\eta = \frac{t_d}{t_c} \quad (8)$$

where t_c and t_d represent the time of charge and discharge, respectively. The columbic efficiency remains above 98% within 5000 cycles. The good contact of the active materials with the current collector can well explain the phenomenon that the peeling off of $Cu(OH)_2$ or CuO from copper foil was not observed during the repetitive charge/discharge cycling. These results implied that the cheap and available $Cu(OH)_2$/Cu-foil electrode has potential application in electrochemical supercapacitors.

For pseudocapacitor, it is well accepted that the capacitance of electroactive material originates from the redox reaction. The reaction kinetics can be evaluated by EIS test. Fig. 7 shows the Nyquist plots of the $Cu(OH)_2$/Cu-foil electrode, $Cu(OH)_2$/Cu-foil electrode after 5000 charge–discharge cycles, CuO/$Cu(OH)_2$/Cu-foil electrode and CuO/Cu-foil electrode measured at open circuit potential in 6.0 mol dm^{-3} KOH solution. All the plots consist of a semicircle at high frequency region and a straight line at low frequency region. A depressed semicircle is observed in the high frequency region, which results from a parallel combination of the charge-transfer resistance (R_{ct}) caused by redox reactions and a constant phase element one (CPE_1). The calculated charge-transfer resistance for $Cu(OH)_2$/Cu-foil electrode is 0.9 Ω cm^{-2}; $Cu(OH)_2$/Cu-foil electrode after 5000 charge–discharge cycles is 2 Ω cm^{-2}; CuO/$Cu(OH)_2$/Cu-foil electrode is 3.6 Ω cm^{-2} and CuO/Cu-foil electrode is 4.6 Ω cm^{-2}. The different resistance is probably owing to the microstructure effect. In the low frequency, the inclined straight line corresponds to Warburg impedance (W_1) related to the diffusion of electrolyte within the nanorods electroactive materials. The straight line part leans more toward the imaginary axis, indicates that the electrode has a good capacitive behavior.[44] EIS results show the $Cu(OH)_2$/Cu-foil electrode has a lower charge transfer resistance and ion diffusion resistance with fast reaction kinetics. It could be considered to be a promising electrode material for pseudocapacitor applications.

Table 2 The lattice parameters of microflower CuO and nanosheet CuO

		Lattice parameters		
Morphology	Crystal system	*a*	*b*	*c*
Microflower CuO	Monoclinic	4.70242	3.40048	5.17389
Nanosheet CuO	Monoclinic	4.6883	3.4229	5.1319

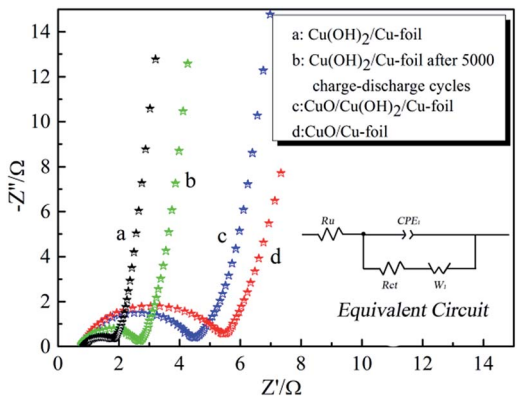

Fig. 7 EIS of the $Cu(OH)_2$/Cu-foil electrode, $Cu(OH)_2$/Cu-foil electrode after 5000 charge–discharge cycles, CuO/$Cu(OH)_2$/Cu-foil electrode and CuO/Cu-foil electrode measured at open circuit potential in 6.0 mol dm^{-3} KOH solution.

3.3. Electrochemical properties of asymmetric supercapacitor

To further demonstrate the potential application of $Cu(OH)_2$ nanowire in supercapacitors, an asymmetric supercapacitor was fabricated by utilising $Cu(OH)_2$/Cu-foil electrode as the positive electrode and AC as the negative electrode (Fig. 8a). The CV curves for AC and $Cu(OH)_2$/Cu-foil electrode at a scan rate of 30 mV s^{-1} in 6 M KOH aqueous solution are shown in Fig. 8b. As can be seen, the potential windows of the AC and $Cu(OH)_2$/Cu-foil electrode are −1.0–0 and 0–0.6 V, respectively. The AC electrode has a nearly rectangular CV curve, limited by H_2 evolution, indicating a typical EDLC behavior since no redox peaks are observed. On the other hand, the CV shape of the $Cu(OH)_2$/Cu-foil displays pseudocapacitance behavior, limited by O_2 evolution, based on a redox mechanism. The total cell voltage can be expressed as the sum of the potential range for the AC and the $Cu(OH)_2$/Cu-foil electrode. Therefore, the cell potential can be as high as 1.6 V in 6 M aqueous KOH electrolyte, which is higher than that of conventional AC-based symmetric supercapacitors in aqueous electrolytes (0.8–1.0 V).

Fig. 8c displays the CV curves of the asymmetric supercapacitor at various scan rates in a potential range of 0–1.6 V. As seen, the CV curve of this supercapacitor exhibited a large current area with broad redox peak, which was the characteristic of the electric double layer capacitance and Faradaic pseudocapacitance. With the increase of scan rate from 5 to 40 mV s^{-1}, the shapes of CV curves do not obviously change, suggesting its good capacitive behavior of the asymmetric supercapacitor. The galvanostatic charge–discharge curves of the asymmetric supercapacitor at different current densities are shown in Fig. 8d. On the basis of the charge–discharge test results, the energy density (E) and power density (P) was calculated according to the following equation:

$$C = \frac{I_d \times \Delta t}{V \times m} \quad (9)$$

$$E = \frac{1}{2} C V^2 \quad (10)$$

$$P = \frac{E}{\Delta t} \quad (11)$$

where I (mA) is the discharge current density, Δt (s) is the discharge time, V (V) is the discharge potential range and m (mg) is the total mass of the active electrode materials. The Ragone plots of the AC//$Cu(OH)_2$/Cu-foil asymmetric supercapacitor cell and AC//AC symmetric supercapacitor are shown in Fig. 8e. The energy density of the AC//$Cu(OH)_2$/Cu-foil supercapacitor reaches 18.3 W h kg^{-1} at a power density of 326 W kg^{-1}, and still remains 14.1 W h kg^{-1} at a power density of 9.8 kW kg^{-1}. The energy densities reduce slowly with increasing power densities. Clearly both the energy and power densities greatly increased compared with the AC//AC symmetric capacitor. These results render $Cu(OH)_2$ promising as one of the most attractive candidates for energy storage. Additionally, the cycling stability of the asymmetric supercapacitor was performed at a constant current density of 0.5 mA cm^{-2} ranging from 0 to 1.5 V for 5000 cycles, as shown in Fig. 8f. The specific capacitance of the asymmetric supercapacitor (AC//$Cu(OH)_2$/Cu-foil) decrease at first and then keep stable. After 5000 cycles, the asymmetric supercapacitor maintains 80% of its original capacitance, which is coincidence with the single $Cu(OH)_2$/Cu-foil electrode (Fig. 6a). These results render it promising as one of the most attractive candidates for energy storage.

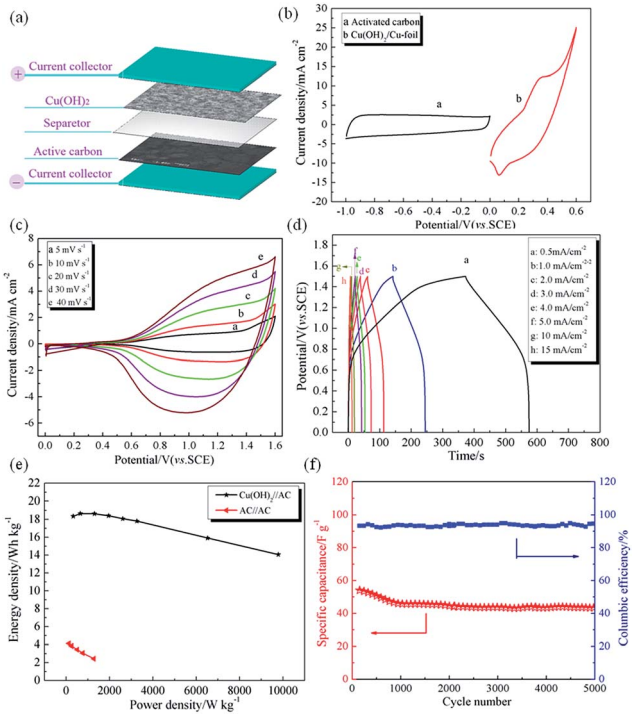

Fig. 8 Schematic illustration of the as-fabricated asymmetric supercapacitor device based on $Cu(OH)_2$/Cu-foil as positive electrode and activated carbon as negative electrode in 6 mol dm^{-3} KOH electrolyte (a); CV curves of $Cu(OH)_2$ and AC electrodes at a scan rate of 10 mV s^{-1} (b); CV curves of $Cu(OH)_2$/Cu-foil//AC asymmetric supercapacitor at different scan rates (c); charge–discharge curves of $Cu(OH)_2$/Cu-foil//AC asymmetric supercapacitor at different current densities (d); Ragone plot related to energy and power densities of the $Cu(OH)_2$/Cu-foil//AC asymmetric supercapacitor and AC//AC symmetric supercapacitors (e); cycle performance of $Cu(OH)_2$/Cu-foil//AC supercapacitor (f).

4. Conclusions

In conclusion, the $Cu(OH)_2$ nanowire arrays, microflower CuO standing on nanowire $Cu(OH)_2$ and uniform flower-like CuO were successfully grown onto copper foil by a facile one-step template-free method to obtain a conducting additive-free and binderless electrode for supercapacitors. The good contact between active materials and the conductive Cu substrate enables their use as integrated electrode for supercapacitors without adding other ancillary materials. The $Cu(OH)_2$/Cu-foil electrode displays the best electrochemical performance with a specific capacitance of 750 F g^{-1} at a current density of 2 mA cm^{-2} (2.86 A g^{-1}) in 6 M KOH electrolyte. Furthermore, fabricating the

asymmetric supercapacitor exhibits a high energy density of 18.3 W h kg^{-1} at a power density of 326 W kg^{-1}.

Acknowledgements

We gratefully acknowledge the financial support of this research by the National Natural Science Foundation of China (21403044), the China Postdoctoral Science Foundation (2014M561332), the Heilongjiang Postdoctoral Fund (LBH-Z13059), the Major Project of Science and Technology of Heilongjiang Province (GA14A101), the Fundamental Research Funds for the Central Universities (HEUCF20151004) and the Project of Research and the Development of Applied Technology of Harbin (2014DB4AG016).

Notes and references

1 P. Simon and Y. Gogotsi, Materials for electrochemical capacitors, *Nat. Mater.*, 2008, **7**, 845–854.
2 D. R. Rolison, J. W. Long, J. C. Lytle, A. E. Fischer, C. P. Rhodes and T. M. McEvoy, *et al.* Multifunctional 3D nanoarchitectures for energy storage and conversion, *Chem. Soc. Rev.*, 2009, **38**, 226–252.
3 G. Wang, L. Zhang and J. Zhang, A review of electrode materials for electrochemical supercapacitors, *Chem. Soc. Rev.*, 2012, **41**, 797–828.
4 P. J. Hall, M. Mirzaeian, S. I. Fletcher, F. B. Sillars, A. J. R. Rennie and G. O. Shitta-Bey, *et al.* Energy storage in electrochemical capacitors: designing functional materials to improve performance, *Energy Environ. Sci.*, 2010, **3**, 1238–1251.
5 X. Zhao, B. M. Sanchez, P. J. Dobson and P. S. Grant, The role of nanomaterials in redox-based supercapacitors for next generation energy storage devices, *Nanoscale*, 2011, **3**, 839–855.
6 T. Xue, C.-L. Xu, D.-D. Zhao, X.-H. Li and H.-L. Li, Electrodeposition of mesoporous manganese dioxide supercapacitor electrodes through self-assembled triblock copolymer templates, *J. Power Sources*, 2007, **164**, 953–958.
7 J. Gamby, P. L. Taberna, P. Simon, J. F. Fauvarque and M. Chesneau, Studies and characterisations of various activated carbons used for carbon/carbon supercapacitors, *J. Power Sources*, 2001, **101**, 109–116.
8 J. Chmiola, G. Yushin, R. Dash and Y. Gogotsi, Effect of pore size and surface area of carbide derived carbons on specific capacitance, *J. Power Sources*, 2006, **158**, 765–772.
9 D. N. Futaba, K. Hata, T. Yamada, T. Hiraoka, Y. Hayamizu and Y. Kakudate, *et al.* Shape-engineerable and highly densely packed single-walled carbon nanotubes and their application as super-capacitor electrodes, *Nat. Mater.*, 2006, **5**, 987–994.
10 C.-M. Yang, Y.-J. Kim, M. Endo, H. Kanoh, M. Yudasaka and S. Iijima, *et al.* Nanowindow-Regulated Specific Capacitance of Supercapacitor Electrodes of Single-Wall Carbon Nanohorns, *J. Am. Chem. Soc.*, 2006, **129**, 20–21.
11 C.-C. Hu, W.-C. Chen and K.-H. Chang, How to Achieve Maximum Utilization of Hydrous Ruthenium Oxide for Supercapacitors, *J. Electrochem. Soc.*, 2004, **151**, A281–A290.
12 C.-C. Hu, K.-H. Chang, M.-C. Lin and Y.-T. Wu, Design and Tailoring of the Nanotubular Arrayed Architecture of Hydrous RuO_2 for Next Generation Supercapacitors, *Nano Lett.*, 2006, **6**, 2690–2695.
13 D.-D. Zhao, S.-J. Bao, W.-J. Zhou and H.-L. Li, Preparation of hexagonal nanoporous nickel hydroxide film and its application for electrochemical capacitor, *Electrochem. Commun.*, 2007, **9**, 869–874.
14 H. Jiang, T. Zhao, C. Li and J. Ma, Hierarchical self-assembly of ultrathin nickel hydroxide nanoflakes for high-performance supercapacitors, *J. Mater. Chem.*, 2011, **21**, 3818–3823.
15 L. Cao, F. Xu, Y. Y. Liang and H. L. Li, Preparation of the Novel Nanocomposite $Co(OH)_2$/Ultra-Stable YZeolite and Its Application as a Supercapacitor with High Energy Density, *Adv. Mater.*, 2004, **16**, 1853–1857.
16 V. Gupta, T. Kusahara, H. Toyama, S. Gupta and N. Miura, Potentiostatically deposited nanostructured α-$Co(OH)_2$: A high performance electrode material for redox-capacitors, *Electrochem. Commun.*, 2007, **9**, 2315–2319.
17 G. Zhu, H. Li, L. Deng and Z.-H. Liu, Low-temperature synthesis of δ-MnO_2 with large surface area and its capacitance, *Mater. Lett.*, 2010, **64**, 1763–1765.
18 O. Ghodbane, F. Ataherian, N.-L. Wu and F. Favier, In situ crystallographic investigations of charge storage mechanisms in MnO_2-based electrochemical capacitors, *J. Power Sources*, 2012, **206**, 454–462.
19 G. Wang, J. Huang, S. Chen, Y. Gao and D. Cao, Preparation and supercapacitance of CuO nanosheet arrays grown on nickel foam, *J. Power Sources*, 2011, **196**, 5756–5760.
20 Y. Li, S. Chang, X. Liu, J. Huang, J. Yin and G. Wang, *et al.* Nanostructured CuO directly grown on copper foam and their supercapacitance performance, *Electrochim. Acta*, 2012, **85**, 393–398.
21 J. Huang, H. Wu, D. Cao and G. Wang, Influence of Ag doped CuO nanosheet arrays on electrochemical behaviors for supercapacitors, *Electrochim. Acta*, 2012, **75**, 208–212.
22 P. M. Kulal, D. P. Dubal, C. D. Lokhande and V. J. Fulari, Chemical synthesis of Fe_2O_3 thin films for supercapacitor application, *J. Alloys Compd.*, 2011, **509**, 2567–2571.
23 X. Xia, Q. Hao, W. Lei, W. Wang, D. Sun and X. Wang, Nanostructured ternary composites of graphene/Fe_2O_3/polyaniline for high-performance supercapacitors, *J. Mater. Chem.*, 2012, **22**, 16844–16850.
24 M.-S. Wu, R.-H. Lee, J.-J. Jow, W.-D. Yang, C.-Y. Hsieh and B.-J. Weng, Nanostructured Iron Oxide Films Prepared by Electrochemical Method for Electrochemical Capacitors, *Electrochem. Solid-State Lett.*, 2009, **12**, A1–A4.
25 A. Ghosh, E. J. Ra, M. Jin, H.-K. Jeong, T. H. Kim and C. Biswas, *et al.* High Pseudocapacitance from Ultrathin V_2O_5 Films Electrodeposited on Self-Standing Carbon-Nanofiber Paper, *Adv. Funct. Mater.*, 2011, **21**, 2541–2547.
26 G. Wee, H. Z. Soh, Y. L. Cheah, S. G. Mhaisalkar and M. Srinivasan, Synthesis and electrochemical properties of

electrospun V_2O_5 nanofibers as supercapacitor electrodes, *J. Mater. Chem.*, 2010, **20**, 6720–6725.

27 R. K. Selvan, I. Perelshtein, N. Perkas and A. Gedanken, Synthesis of Hexagonal-Shaped SnO_2 Nanocrystals and SnO_2@C Nanocomposites for Electrochemical Redox Supercapacitors, *J. Phys. Chem. C*, 2008, **112**, 1825–1830.

28 W. Chen, R. B. Rakhi, L. Hu, X. Xie, Y. Cui and H. N. Alshareef, High-Performance Nanostructured Supercapacitors on a Sponge, *Nano Lett.*, 2011, **11**, 5165–5172.

29 Y.-C. Chen, Y.-K. Hsu, Y.-G. Lin, Y.-K. Lin, Y.-Y. Horng and L.-C. Chen, *et al.* Highly flexible supercapacitors with manganese oxide nanosheet/carbon cloth electrode, *Electrochim. Acta*, 2011, **56**, 7124–7130.

30 D. P. Dubal, G. S. Gund, R. Holze and C. D. Lokhande, Mild chemical strategy to grow micro-roses and micro-woolen like arranged CuO nanosheets for high performance supercapacitors, *J. Power Sources*, 2013, **242**, 687–698.

31 X. Zhang, L. Yu, L. Wang, R. Ji, G. Wang and B. Geng, High electrochemical performance based on ultrathin porous CuO nanobelts grown on Cu substrate as integrated electrode, *Phys. Chem. Chem. Phys.*, 2013, **15**, 521–525.

32 Y.-K. Hsu, Y.-C. Chen and Y.-G. Lin, Characteristics and electrochemical performances of lotus-like CuO/$Cu(OH)_2$ hybrid material electrodes, *J. Electroanal. Chem.*, 2012, **673**, 43–47.

33 K. V. Gurav, U. M. Patil, S. W. Shin, G. L. Agawane, M. P. Suryawanshi and S. M. Pawar, *et al.* Room temperature chemical synthesis of $Cu(OH)_2$ thin films for supercapacitor application, *J. Alloys Compd.*, 2013, **573**, 27–31.

34 C. Zhou, Y. Zhang, Y. Li and J. Liu, Construction of High-Capacitance 3D CoO@Polypyrrole Nanowire Array Electrode for Aqueous Asymmetric Supercapacitor, *Nano Lett.*, 2013, **13**, 2078–2085.

35 M. Yu, T. Zhai, X. Lu, X. Chen, S. Xie and W. Li, *et al.* Manganese dioxide nanorod arrays on carbon fabric for flexible solid-state supercapacitors, *J. Power Sources*, 2013, **239**, 64–71.

36 L. Yang, S. Cheng, Y. Ding, X. Zhu, Z. L. Wang and M. Liu, Hierarchical Network Architectures of Carbon Fiber Paper Supported Cobalt Oxide Nanonet for High-Capacity Pseudocapacitors, *Nano Lett.*, 2011, **12**, 321–325.

37 J. Huang, P. Xu, D. Cao, X. Zhou, S. Yang and Y. Li, *et al.* Asymmetric supercapacitors based on β-$Ni(OH)_2$ nanosheets and activated carbon with high energy density, *J. Power Sources*, 2014, **246**, 371–376.

38 Y. Liu, Y. Qiao, W. Zhang, P. Hu, C. Chen and Z. Li, *et al.* Facile fabrication of CuO nanosheets on Cu substrate as anode materials for electrochemical energy storage, *J. Alloys Compd.*, 2014, **586**, 208–215.

39 B. Vidhyadharan, I. I. Misnon, R. A. Aziz, K. P. Padmasree, M. M. Yusoff and R. Jose, Superior supercapacitive performance in electrospun copper oxide nanowire electrodes, *J. Mater. Chem. A*, 2014, **2**, 6578–6688.

40 J.-B. He, D.-Y. Lu and G.-P. Jin, Potential dependence of cuprous/cupric duplex film growth on copper electrode in alkaline media, *Appl. Surf. Sci.*, 2006, **253**, 689–697.

41 M. Jayalakshmi and K. Balasubramanian, Cyclic Voltammetric Behavior of Copper Powder Immobilized on Paraffin Impregnated Graphite Electrode in Dilute Alkali Solution, *Int. J. Electrochem. Sci.*, 2008, **3**, 1277–1287.

42 L. M. Abrantes, L. M. Castillo, C. Norman and L. M. Peter, A photoelectrochemical study of the anodic oxidation of copper in alkaline solution, *J. Electroanal. Chem. Interfacial Electrochem.*, 1984, **163**, 209–221.

43 S. Nakayama, A. Kimura, M. Shibata, S. Kuwabata and T. Osakai, Voltammetric Characterization of Oxide Films Formed on Copper in Air, *J. Electrochem. Soc.*, 2001, **148**, B467–B472.

44 Y. Gao, S. Chen, D. Cao, G. Wang and J. Yin, Electrochemical capacitance of Co_3O_4 nanowire arrays supported on nickel foam, *J. Power Sources*, 2010, **195**, 1757–1760.

45 Y. X. Zhang, M. Huang, F. Li and Z. Q. Wen, Controlled Synthesis of Hierarchical CuO Nanostructures for Electrochemical Capacitor Electrodes, *Int. J. Electrochem. Sci.*, 2013, **8**, 8645–8661.

46 X. Zhang, L. Yu, L. Wang, R. Ji, G. Wang and B. Geng, High electrochemical performance based on ultrathin porous CuO nanobelts grown on Cu substrate as integrated electrode, *Phys. Chem. Chem. Phys.*, 2013, **15**, 521–525.

47 B. Heng, C. Qing, D. Sun, B. Wang, H. Wang and Y. Tang, Rapid synthesis of CuO nanoribbons and nanoflowers from the same reaction system, and a comparison of their supercapacitor performance, *RSC Adv.*, 2013, **3**, 15719–15726.

48 Y. X. Zhang, M. Huang, M. Kuang, C. P. Liu, J. L. Tan, M. Dong, Y. Yuan, X. L. Zhao and Z. Wen, Facile Synthesis of Mesoporous CuO Nanoribbons for Electrochemical Capacitors Applications, *Int. J. Electrochem. Sci.*, 2013, **8**, 1366–1381.

